Hindawi
Journal of Electrical and Computer Engineering
Volume 2022, Article ID 2971960, 19 pages
https://doi.org/10.1155/2022/2971960

Research Article

Application of Data-Driven Tuned Fuzzy Inference System for Static Equivalencing of Power Systems with High Penetration of Renewable Energy

Engidaw Abel Hailu,[1] **George Nyauma Nyakoe**,[2] **and Christopher Maina Muriithi**[3]

[1]*Pan African University Institute for Basic Sciences Technology and Innovation (PAUSTI), Juja, Kenya*
[2]*Jomo Kenyatta University of Agriculture and Technology (JKUAT), Juja, Kenya*
[3]*Murang'a University of Technology (MUT), Murang'a, Kenya*

Correspondence should be addressed to Engidaw Abel Hailu; enabel02@gmail.com

Received 21 July 2022; Revised 31 August 2022; Accepted 6 September 2022; Published 23 September 2022

Academic Editor: B. Rajanarayan Prusty

To reduce the complexity of multiarea power systems during power flow study and security assessment, equivalencing of external power systems is essential. In this paper, external power systems are modeled as adaptive loads representing the tie-line flows varying with system operating conditions. The fuzzy inference system tuned by hybrid genetic-simulated annealing (HGSA-FIS) is proposed to predict the active and reactive power of adaptive loads from forecasted renewable energy (RE) generation and loads demand. The performance of proposed equivalent has been evaluated with an RTS-GMLC by comparing the power flow results in the internal system before and after equivalencing under varying RE and load demand scenarios. The results demonstrate the robustness of HGSA-FIS-based equivalent under varying RE generation and load demand. Furthermore, the proposed equivalent performs close to ANN-based equivalent and outperforms ANFIS-based equivalent. To practically implement the proposed approach, the neighboring system operators are required to exchange only the forecast data of RE generation and load demand, and the equivalent needs to be updated upon major grid changes.

1. Introduction

The electric power networks are complex infrastructures that are continuously evolving worldwide to provide reliable and affordable energy supply to the consumers. One evidence of this evolution is the increase of the interconnection of several power networks with independent operators [1]. To overcome the economic and technical challenges faced by independent power grids and achieve economic operation by sharing unevenly distributed resources and infrastructure, and bilateral electric power trading, power system interconnection becomes a common practice around the world [2, 3]. Interconnection among power systems managed and controlled by different operators along with the increasing penetration of renewable energy-based generation brings about new challenges into the power system, such as increased complexity, uncertainty, interarea oscillation, and increased difficulty to real-time power system security evaluation and control [4–8].

In such large multiarea interconnected power systems, the control center of each area is responsible for security monitoring, analysis, and control of its part of the whole system [9, 10]. However, the security assessment and control decision can be made based on the analysis of the whole system as possible disturbances or contingencies beyond ones control area (external system) may potentially affect the secure operation of the control area system (internal system) [11–13].

To incorporate the impact of disturbances from an external power system in the security analysis of internal power system, either complete external power system information or external equivalent network model is required. In practical multiarea power systems, because of the technical issues or the commercial confidentiality, the required

network and online grid operation data outside one's control area is difficult to obtain [14–16]. Consequently, security analysis based on multiple power flows for all credible outages in the whole system, at frequent intervals, becomes an impossible task [17, 18]. Hence, the modeling of external system becomes one of the most important issues in the security assessment of multiarea power systems [19]. This issue may arise both in operational planning and real-time system operation [10]. Therefore, the updated equivalent model of external systems together with detailed model of internal system is required to perform any kind of power system analysis in the internal system [8, 11]. The reduced power system with the external equivalent has some advantages, such as fast online computational performance and better database maintenance [20–23].

Depending on the purpose of the equivalent model, power grid equivalent techniques can be classified into dynamic and static [23]. A dynamic equivalent is required to represent the dynamics in the external power grid in transient, voltage, and frequency stability studies of the internal power system [24]. Static equivalent is required to represent the disturbances, such as change in power flows and bus voltage, and its applications are mainly in the area of power flow analysis and static security assessment of large multiarea power systems. In this paper, the word "equivalent" mainly refers to grid static equivalent targeted to perform static security assessment. To ensure the simplified equivalent system, maintain the static characteristics of the original system. The power flow of the internal system before and after the equivalence remains unchanged [8, 25].

A variety of equivalent models for steady state power system analysis has been developed. Most of the equivalent models are based on the linear approximation of nonlinear power system [26, 27]. Ward, extended ward, and Ward-PV are popular equivalencing approaches [9, 13, 14, 28], which are available in power system software tools like DIgSILENT power factory [29], power world simulator, [30] and Pandapower [31]. In the simple ward equivalent model, load and generator buses are eliminated from the reduced portion of network, and the external system is modeled as a set of equivalent impedance, shunts, and power injections attached to the boundary buses. Gaussian matrix elimination or reduction procedure is followed to reduce the admittance matrix of the network. Nevertheless, it does not provide accurate results for static security study [32, 33]. In the extended ward method, the accuracy of the simple ward is improved by adding reactive power support. In Ward-PV equivalent, the PV (generator) buses of the external system are retained, and it performed better than ward and extended ward approaches for static security analysis. To reduce the number of generators in the Ward-PV equivalent model, coherency-based aggregation of generator nodes is suggested in [9], and the resulting equivalent model is called reduced the Ward-PV model.

To minimize the load flow errors associated with Ward and its variants, the radial equivalent and independent (REI) approach has been introduced [23, 34, 35]. In this approach, the power and current injection in external areas are aggregated to a fictitious bus. The number of fictitious buses created depends on the number of desired generators and loads [36]. Then, Gaussian elimination is used to reduce the grid resulting from power aggregation. In the REI approach, an adaptation to other operating conditions can be made with the simple scaling of the original operating point of the aggregated devices only when the power changes in the external areas are not large [23].

The aforementioned conventional grid equivalencing techniques require not only the knowledge of complete topology and network parameters of the external system but also recalculation of the grid equivalent networks and power injections every time the grid state changes in one of the connected systems [8, 23, 25, 37], which is not practical for modern power systems dominated by various renewable energy based generators (REGs) with frequent variations [15, 16, 32]. The power system operating condition is continuously changing throughout the day as a result of demand and generation variations. Hence, the tie-line flows and resulting boundary power injections would need to be updated from time to time. This issue becomes critical for power systems dominated by renewable energy resources and significant load perturbation.

The goal of adaptive grid equivalencing is to take into account the impact of the external generation and load variations and other disturbances on the study of internal power systems as accurately as possible [8]. For modern power systems with intermittent generation because of renewable energy resources (RERs) and varying load demand, unless the external equivalent is updated frequently, it leads to misleading security assessment results [10]. Once developed and tested, the external static equivalent model would be connected to an internal power system to perform the required power system steady state analysis like load flow study or security assessment with sufficient accuracy and reduced computational effort in a short time [14, 25].

Equivalent models based on artificial neural network (ANN) have been developed and tested for different multiarea power systems [8, 22, 23, 26, 27, 37–39]. As demonstrated in [8, 23], the ANN equivalent model provides more accurate equivalences than the REI models with limited grid data in a short time.

Power system operation is full of uncertainties derived mainly from RERs and demand forecasting and measurement errors [40]. Hence, fuzzy logic systems are suitable techniques to make a generalized prediction of the line flows. Fuzzy inference system (FIS) enhanced with learning capability can be designed to learn from the past power system operating conditions and be applied to predict tie-line flows in the future. When a significant change occurs to the power system network, the FIS model may need to be updated to incorporate the network changes. Interpretability, transparency, and ability to handle uncertainties and measurement errors are some advantages of FIS over other machine learning techniques [41].

In this paper, the external area system is modeled as adaptive load equivalent to the tie-line flows whose value depends on the generation and loads in the system. By exploring the relationship between inputs (RE generation and load demand) and outputs (tie-line flows), a fuzzy

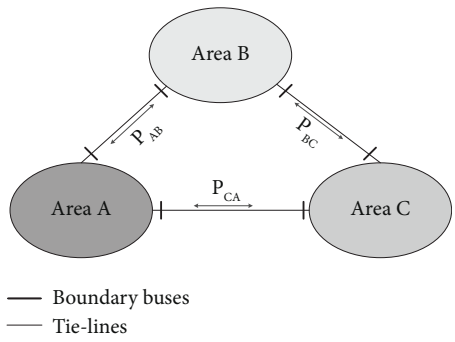

Figure 1: Three-area power system.

inference system (FIS) is developed. The FIS model is the required external power system equivalent model. To minimize the prediction error of the FIS model, the hybrid genetic-simulated annealing (HGSA) optimization algorithm is proposed to tune the antecedent and consequent parameters. Its performance has been compared with artificial neural network (ANN) and adaptive neuro-fuzzy inference system (ANFIS). The proposed prediction model can be adapted to new operating scenarios of the power system by simply retraining the model with new sample scenarios. The key contributions of this paper are as follows:

(i) The neighborhood component analysis for regression (NCAR) algorithm is employed to reduce the number of input attributes (features) so that only more informant variables are used and model training costs are significantly reduced. As a result, the active power generation and demand of only few REGs and loads, respectively, at selected locations have been used to build the external equivalent, and no detail network data is required.

(ii) An adaptive equivalencing approach that can predict the tie-line flows from only limited RE-generation and load demand data obtained from internal and external area power systems is proposed. Only foretasted REG output power and load demand data are required to obtain the static equivalent.

(iii) An HGSA-based FIS model is implemented, and its parameters are tuned to predict the tie-line active and reactive power flows between neighboring power systems in the three-area power system under varying power system operating conditions.

The remaining of this paper is organized as follows: Section 2 discusses the theoretical fundamentals of grid equivalencing and fuzzy inference system. The materials and methods, including a brief description of the case study system and operating scenarios, the static representation of external power system, the HGSA-FIS model development, and performance evaluation metrics, are presented in Section 3. Section 4 presents the results and discussion. Finally, in Section 5, conclusions are drawn.

2. Theoretical Background

2.1. Static Grid Equivalencing. A three-area power system is shown in Figure 1. In power system planning and operation, the part of the whole power system under investigation/study is considered *internal*, while the remaining part of the whole system is considered *external* [14, 25]. As shown in the figure, for the operator responsible for Area *A*, the other area power systems (Area *B* and Area *C*) are considered external. The end nodes of the interconnecting tie lines are called boundary buses.

The interaction between the connected area power systems is reflected by the power exchange at the interconnecting tie-lines [14, 23]. From the perspective of operator responsible for Area *A*, static equivalents of Area *B* and Area *C* can be represented as load or generator equivalent to the tie-line flows between Area *A* and respective grids, as shown in Figure 2.

Provided that the grid network remains significantly unchanged, the relationship between grid states and tie-line flows remains the same [23]. Two questions should be answered in this regard, which are as follows: (1) which grid parameters can be used to describe the grid states? (2) How can the tie-line flows be estimated? The choice of grid parameter depends whether the required measurement or forecasted data is available. FIS can be implemented to map the grid states to adaptive load/generation representing the tie-line flows [26] as presented as follows:

$$f: X \longrightarrow Y, \tag{1}$$

where f is the FIS model, X represents the grid parameters describing grid states, and Y represents the active and reactive power values of adaptive load/generation. The parameters describing the grid states can be buses' voltage, line flows, generator outputs, and loads' demand. Because of data unavailability in practical scenarios, the selected grid parameters consist of the power output of REGs and active and reactive power demand of the load. As shown in Figure 3, to successfully map grid states to adaptive load/generation, the FIS model passes through the training or tuning process using the historical input-output dataset and then applied for the prediction of active and reactive power values of adaptive load/generation for unseen grid states.

2.2. Fuzzy Inference System Fundamentals. Fuzzy inference is a process of mapping the inputs to the outputs using fuzzy logic, which is contained by IF-THEN rules, membership functions, and fuzzy logical operations [42]. As shown in Figure 4, the FIS model has the following five functional blocks: fuzzifier, database, rule base, fuzzy inference engine, and defuzzifier [43].

A fuzzifier transforms a crisp input into a fuzzy value between 0 and 1 by determining the degree of membership of each input to each of the appropriate fuzzy sets. Membership functions (MF) are used in the transformation. A database defines linguistic variables or terms associated with each input variable used in fuzzy rules. Rule base is a set of if-then rules representing expert knowledge or input-output

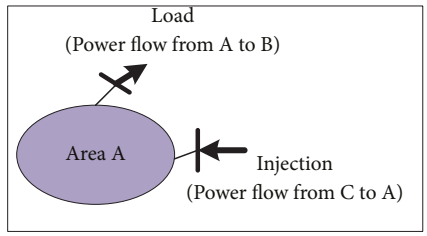

Figure 2: Representation of tie-line flows as load or injection.

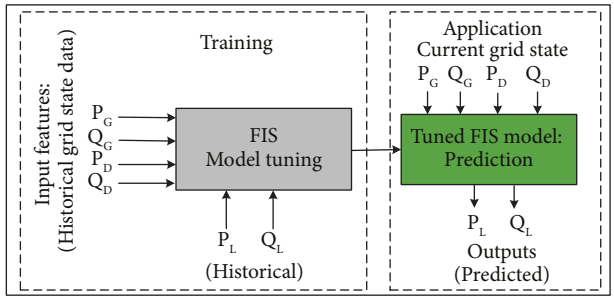

Figure 3: Fuzzy inference system for mapping inputs (generation & load) and outputs (line flows).

relationship of experimental data. Fuzzy inference engine computes the rules firing strengths from fuzzy inputs to infer knowledge from the database and rule base. The process of fuzzy inference involves all the membership functions, fuzzy logic operators, and if–then rules. A defuzzifier translates inferred knowledge into a rule action (crisp output).

The i^{th} rule of a Takagi-Sugeno-Kang (TSK) FIS model with K rules and N input variables $(x_1, \ldots, x_N)$ and a single output y can be described as follows [41, 44]:

Rule i: if $(x_1$ is $A_i^1)\ldots$and $(x_j$ is $A_i^j)\ldots$ and $(x_N$ is $A_i^N)$, then $(y_i = p_i^1 x_1 + \cdots + p_i^j x_j + \cdots + p_i^N x_N + r_i)$ where A_i^j is the fuzzy set of j^{th} input in the antecedent of i^{th} rule, while p_i^j and r_i are real constants called consequent parameters corresponding to the j^{th} input and i^{th} rule. $i = 1, 2, \ldots, K$ and $j = 1, 2, \ldots, N$.

The crisp output y is computed by the weighted average of each rule output, and it can be expressed as follows [45]:

$$y = \frac{\sum_{i=1}^{K} w_i y_i}{\sum_{i=1}^{K} w_i}, \tag{2}$$

where y_i is the output rule i and w_i the rule firing strength, which is the matching degree between the antecedent part of the i^{th} rule and the current input [42], and it can be obtained from the product of the degree of membership for each current input as follows:

$$w_i = \prod_{j=1}^{N} \mu_{A_i^j}(x_j), \tag{3}$$

where $\mu_{A_i^j}(x_j)$ is the degree of membership associated with fuzzy set A_i^j evaluated at input x_j. A Gaussian MF used in this paper can be expressed as follows:

$$\mu_{A_i^j}(x_j) = e^{-\frac{1}{2}\frac{(x_j - c_i)^2}{\sigma_i}}, \tag{4}$$

where c and σ are the mean and standard deviation of the MF. At the FIS model development stage, the optimization approaches deal with the problem of designing and optimizing a fuzzy rule base and the parameters of membership functions (MFs) using input-output data to minimize the prediction error. The simultaneous optimization of the rule base and parameters of input and output MFs is not convenient [46]. Therefore, the optimization of the FIS model consists of three stages, which are as follows: rule base tuning, optimization of input MF parameters, and optimization of linear output function parameters.

Rule base optimization is accomplished for the coarse tuning of the model followed by the fine tuning of the model by optimizing the input MF parameters and linear output parameters, given a predefined rule base. Various approaches have been proposed for the development, tuning, and optimization of fuzzy models. Some of these are inductive learning [47, 48], descent methods, neural networks [49], clustering technique [50], genetic algorithms [46], and simulated annealing [51, 52]. In this paper, hybrid genetic-simulated annealing (HGSA) has been applied to solve the optimization problem formulated to minimize the FIS prediction error.

2.3. Hybrid Genetic-Simulated Annealing. Genetic algorithm (GA) and simulated annealing (SA) represent two powerful stochastic optimization methods with complementary strengths and weaknesses [53]. For a population-based approach like GA, finding optima is achieved in a short time. SA performs better than GA in finding a global optimal solution. Nevertheless, GA has poor nearby pursuit capacity, and SA is a computationally slow process. To overcome the shortcomings of GA and SA, the hybrid between GA and SA called hybrid genetic-simulated annealing (HGSA) is proposed to build a robust algorithm [54, 55]. HGSA not only avoids the problem of the premature convergence of GA but also increases the computational speed of SA [56, 57]. The fast and global parallel searching ability of GA is retained, and the diversity is improved by SA state transition [56]. A more detailed explanation and flowchart of the HGSA algorithm is provided in Section 3.3.

3. Materials and Methods

3.1. Case Study System. In this paper, the reliability test system of grid modernization lab consortium (RTS-GMLC) [58], updated in 2019 from IEEE reliability test system-96 (IEEE RTS-96) [59], is used as a case study system. The RTS-GMLC ia a three-area test system that has been updated by introducing a generation mix that is more representative of modern power systems by removing several nuclear- and oil-based generating units and adding natural gas, hydro, wind, solar photovoltaic (PV), and concentrating solar power (CSP). The grid data is available at GitHub Repository

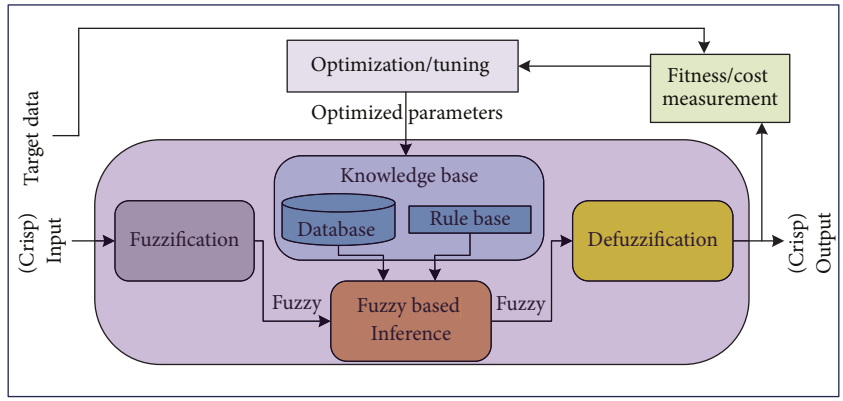

Figure 4: Architecture of fuzzy inference system with optimization or tuning.

[60]. The overall network of the three-area power grid drawn using Pandapower is shown in Figure 5. The power grid is divided into three areas (Area *A*, Area *B*, and Area *C*) using dashed red lines. The part of the three-area power system considered internal in this paper is Area A, which consists of buses 101–124, and the other areas are considered external. As shown in the figure, Area *A*/Area *B* is interconnected to Area *C* by one tie-line (L102 and L103, respectively), while Area *A* and Area *B* are interconnected by three tie-lines (L10, L18, and L35) connected to different substations. Buses B107, B113, B121, and B123 are boundary buses from the side of Area A.

The loads distributed at different buses of the system are supplied with 154 generators, of which 81 are REGs based on hydro, wind, and solar, and 73 generators based on coal, oil, natural gas, and nuclear power. The total connected and peak loads are 8.55 GW and 8.00 GW, respectively. The maximum installed generation capacity is 15 GW, of which 42.82% is from REGs.

There are 3×200MVAR synchronous condensers, one at each area installed to provide reactive power support to the system, and each area has its own slack generator.

The five-day profile of the active and reactive power demand of the system loads and active power output of REGs sampled at 5 mins interval is shown in Figure 6(a). As observed in the figure, the REG generation output variation is much noticeable than the load demand variation. This variability of REG generation and load demand causes a significant variation of active and reactive power flows through tie-lines L10, L18, L35, and L102, as shown in Figures 6(b) and 6(c). P_n and Q_n for $n = (10, 18, 35, 102)$ are the active and reactive power flows of respective tie-lines.

As observed in Figure 6, there is a strong dependency of tie-line flows on REG power output and load demand. In this paper, the dependency of tie-line flows on REG output and load demand is explored and has been used to develop FIS that can make the prediction of tie-line flows from the forecast data of REG output and loads demand.

3.2. Representation of External Power System. Considering the three-area power system shown in Figure 5 and assuming Area *A* as a study (internal) power system and Area *B* and Area *C* as external power systems, the reduced power

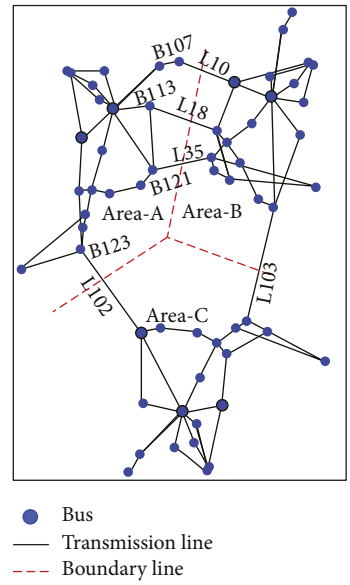

Figure 5: Case study system: reliability test system of grid modernization lab consortium (RTS-GMLC).

system can be represented as shown in Figure 7. A comparison of the number of components involved in the full three-area system against those ones in the reduced is provided in Table 1.

As shown in Figure 7, the system complexity is reduced significantly since about two-third of the power system is replaced by adaptive loads equivalent to active and reactive power flows of four tie-lines. With reduced system, no detailed external network data is required to carry out the power flow analysis or security assessment of the internal system.

In the figure, blocks FISXP and FISXQ predict P_X and Q_X, respectively, for $X = (10, 18, 35, 102)$, from the forecasted values of the output power of REGs (P_G), active power demand (P_D), and reactive power demand (Q_D) of the loads distributed throughout the three-area power system. FIS10P, FIS10Q, FIS18P, FIS18Q, FIS35P, and FIS35Q represent Area *B*, and FIS102P and FIS102Q represent Area *C*. The relationship between inputs and outputs of FIS blocks can be expressed as follows:

$$\begin{pmatrix} P_{10} \\ Q_{10} \\ P_{18} \\ Q_{18} \\ P_{35} \\ Q_{35} \\ P_{102} \\ Q_{102} \end{pmatrix} = \begin{pmatrix} f_1\left(P_{G1}, \ldots, P_{Gng}, P_{D1}, \ldots, P_{Dnd}, Q_{D1}, \ldots, Q_{Dnd}\right) \\ f_2\left(P_{G1}, \ldots, P_{Gng}, P_{D1}, \ldots, P_{Dnd}, Q_{D1}, \ldots, Q_{Dnd}\right) \\ f_3\left(P_{G1}, \ldots, P_{Gng}, P_{D1}, \ldots, P_{Dnd}, Q_{D1}, \ldots, Q_{Dnd}\right) \\ f_4\left(P_{G1}, \ldots, P_{Gng}, P_{D1}, \ldots, P_{Dnd}, Q_{D1}, \ldots, Q_{Dnd}\right) \\ f_5\left(P_{G1}, \ldots, P_{Gng}, P_{D1}, \ldots, P_{Dnd}, Q_{D1}, \ldots, Q_{Dnd}\right) \\ f_6\left(P_{G1}, \ldots, P_{Gng}, P_{D1}, \ldots, P_{Dnd}, Q_{D1}, \ldots, Q_{Dnd}\right) \\ f_7\left(P_{G1}, \ldots, P_{Gng}, P_{D1}, \ldots, P_{Dnd}, Q_{D1}, \ldots, Q_{Dnd}\right) \\ f_8\left(P_{G1}, \ldots, P_{Gng}, P_{D1}, \ldots, P_{Dnd}, Q_{D1}, \ldots, Q_{Dnd}\right) \end{pmatrix}, \tag{5}$$

where f_1-f_8 represent the FIS prediction models, P_{Gi} is the active power output of generator i, P_{Di} and Q_{Di} are the active and reactive power demand of load point i, respectively, and ng and $n\ d$ are the number of REGs and loads, respectively. To make a successful prediction of tie-line flows, FIS prediction models are designed and tuned using the HGSA algorithm.

3.3. HGSA-FIS Model Development. The FIS models that are used to predict the active and reactive power flows across tie-lines for unseen operating conditions have been developed from historical input-output dataset. The procedure followed to develop the FIS model is shown in the flow chart presented in Figure 8.

The process starts with collecting the network data for the three-area power system to be reduced. The network is modeled with Pandapower, a Python-based open source power system analysis tool. To generate input-output dataset, time-series REG output and load demand data obtained from [60] have been used. After the generation of input-output dataset using power flow analysis, feature selection has been carried out to select more informative attributes. Feature selection helps to remove a significant portion of input variables. The dataset is then split into train-test sets. The training data has been used to generate the initial FIS model rule base and input and output MF parameters. The initial FIS model is generated using Fuzzy C-means (FCM) clustering. The input MF parameters and linear output function parameters of initially generated FIS model are used to initialize the FIS tuning using HGSA. When the tuning is finished, the resulting FIS model is checked with an unseen dataset. If the performance of the FIS model is found unsatisfactory during testing, the ones that can be adjusted are as follows: (1) the threshold of weights of features to be retained, (2) number of clusters, and (3) parameters in HGSA like cross-over rate, mutation rate, temperature, and cooling rate. A more detailed explanation of the major blocks presented in the flowchart is given in the subsequent subsections.

3.4. Dataset Generation and Feature Selection. Before the FIS model is used for prediction, it should be trained very well so that it can make generalizations for the unseen operating conditions of the power system. To make a reliable prediction, the FIS model should be sufficiently trained with the dataset, which covers as many operating conditions as possible. In practical power systems, the training set is obtained from historical data. In this paper, the training dataset is generated by running time series power flow analysis of the whole multiarea power system using Pandapower. For each power flow analysis, the active and reactive power flows across the tie-lines and respective REGs power output and load demand are recorded throughout the time-series power flow simulation. The number of instances (power flow simulations) is limited to 1440 grid states because of the time and resource limitation required to solve power flow simulations. Eight datasets are generated for training eight FIS models shown in Figure 7.

Since the same operating conditions have been used to generate eight outputs, the initial number and category of input attributes are the same for each dataset. In FIS modeling, the proper choice of input variables has a paramount importance [50]. Initially, there are 183 input features (81 P_G's + 51 P_D's + 51 Q_D's). The number of parameters required for FIS tuning highly depends on the number of input features and rules [61]. For an FIS model with N input features and K rules, the number of tunable parameters becomes $M = 2K(2N + 1)$. Therefore, for each additional input variable, there will be a $4K$ increase in the number of tunable parameters, implying the necessity of feature reduction during model building.

The main benefits of feature selection are to improve prediction performance, provide faster and more cost-effective predictors, provide a better understanding of the data generation process [62], and ease the task of the operator by reducing the size of data that should be obtained from internal and external area power systems.

Prior to this, the standard feature selection algorithm was implemented to filter out irrelevant features. Common sense approaches listed subsequently have been implemented to reduce the number of input features, which are as follows: (1) a variable that does not change its value throughout the time series is removed. (2) If two or more features have similar values or are linearly dependent, only one is retained. The application of these techniques has reduced the number of features from 183 to 115 (i.e., 40.41%

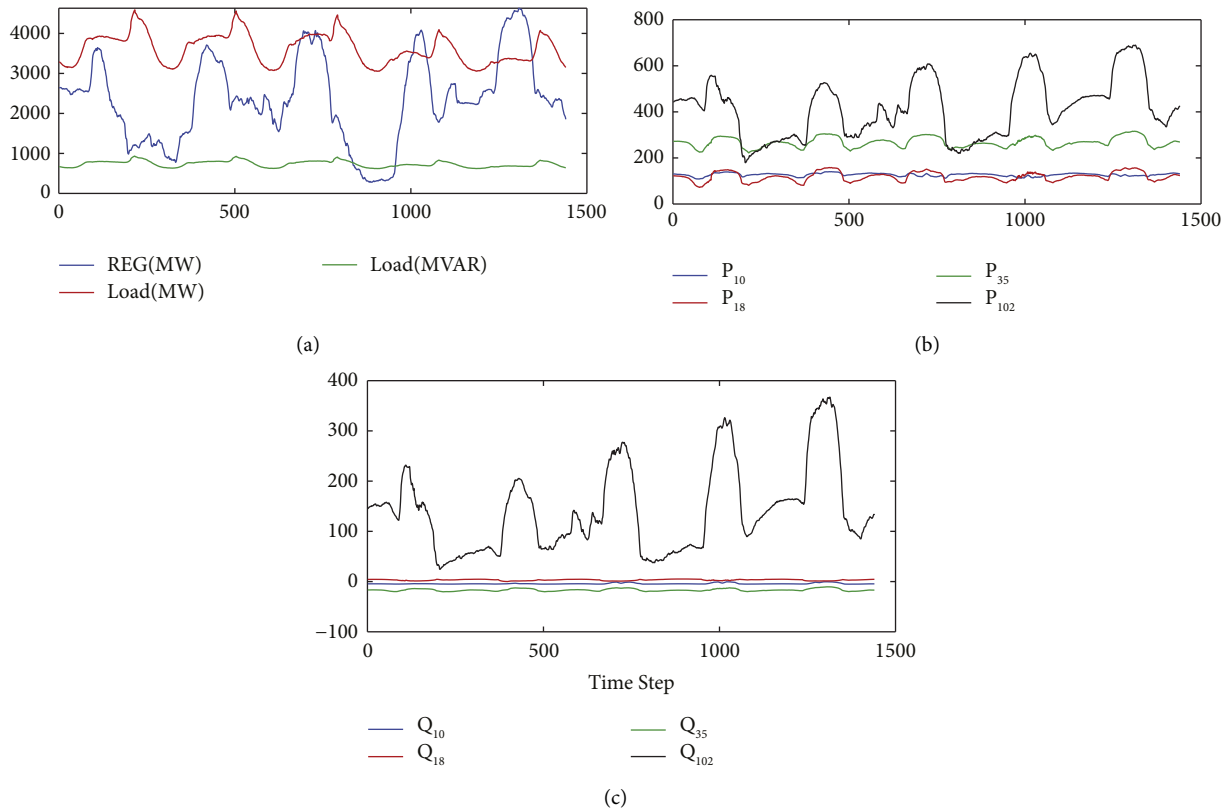

Figure 6: Time series profile of (a) DER generation output (MW) and load demand (MW/MVAR), (b) tie-lines's active power flow (MW), and (c) tie-lines's reactive power flow (MVAR).

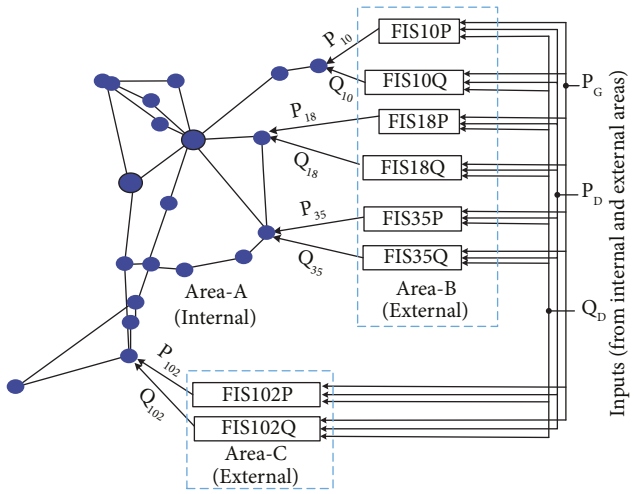

Figure 7: Representation of external areas by dependent loads.

Table 1: Comparison of original and reduced system with external equivalents.

No.	Component	Original system	Reduced system
1	Buses	73	24
2	Generators	153	50
3	Lines	103	32
4	Transformers	16	5
5	Loads	51	17

reduction), thus simplifying the task for the feature selection algorithm. The remaining 115 features consist of 64 P_G's and 51 P_D's. Yet, the FIS model training using 115 input features is computationally cumbersome. Features that highly influence each tie-line active and reactive power flows should be selected carefully.

Among the commonly used feature selection techniques, the neighborhood component analysis for regression (NCAR) has been implemented in this work to select the most relevant features. NCAR is a nonparametric method for selecting features with the goal of maximizing prediction accuracy. It uses the gradient ascent technique to maximize the expected leave-one-out regression accuracy with a regularization term of the learning model. A more detailed formulation of NCA is available in [63]. Features selected to train the FIS model for predicting P_L's may not be similar to features selected to train the FIS model used to predict Q_L's even for the same tie-line. Table 2 presents the number and category of selected features for training the FIS models of active and reactive power flows of tie-lines under consideration.

The overall feature selection process reduces the number of input features by more than 84.7%. As shown in the table, most of the selected features are REG active power outputs (P_G's). Among the selected REGs, the majority are based on solar, followed by wind and hydro. It is because of the high variability of power output from solar PV plants, as compared to wind and hydro generators. The selected REGs and loads are distributed throughout the three-area power

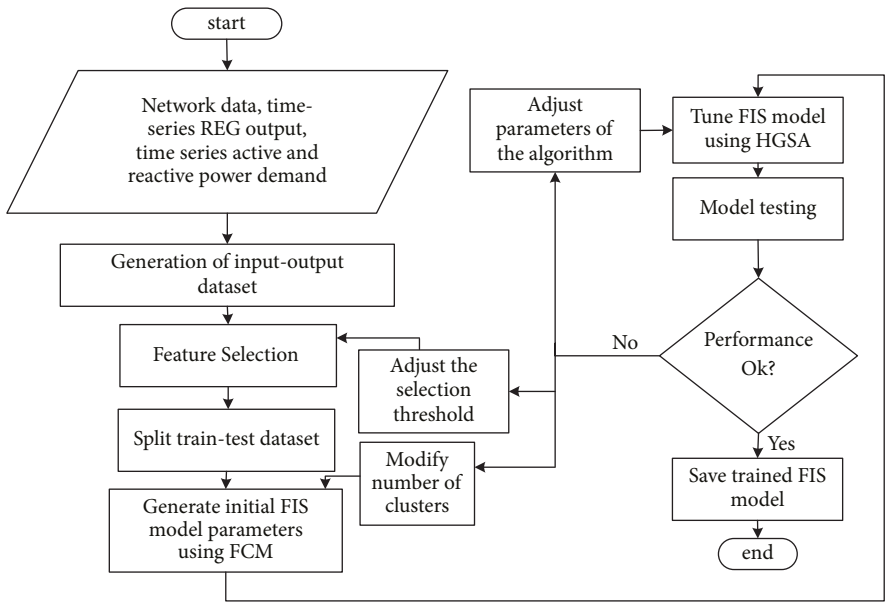

Figure 8: Overall procedure of FIS model training and testing.

Table 2: Number and category of selected features.

Target	Number of selected input features					Overall reduction (%)
	REGs			Loads	Total	
	Solar	Wind	Hydro			
P_{10}	11	4	1	3	19	89.6
Q_{10}	2	4	1	4	11	92
P_{18}	13	3	2	3	21	88.5
Q_{18}	8	4	1	6	19	89.6
P_{35}	11	1	1	2	15	91.8
Q_{35}	9	4	1	3	17	90.7
P_{102}	16	4	1	2	23	84.7
Q_{102}	19	4	0	3	26	85.8

system. In case of features selected to predict P_{10} (active power flow from Area A to Area B through tie-line L10), 44.4%, 16.7%, and 38.9% of the features are physically located in Area A, Area B, and Area C, respectively. Therefore, an operator responsible for Area A requires REG generation and load demand forecast data from the neighboring power grids. No detailed grid network information is required to predict the tie-line flows.

3.5. Training, Validation, and Test Dataset. The dataset required for model training is based on the time-series profile of REG active power output and load demand of the RTS-GMCL system for five consecutive days in a five-minute interval (total samples = 1440). The dataset is divided into train-test partitions using cross-validation by holding out 30% of samples as testing data, and the remaining 70% are used for model training and validation. To overcome the data over-fitting problem during training, a K-fold cross-validation approach has been implemented. After many trials, the number of folds is determined to be six ($K = 6$). The training data is randomly shuffled and then divided into six partitions, as shown in Figure 9. The training-validation

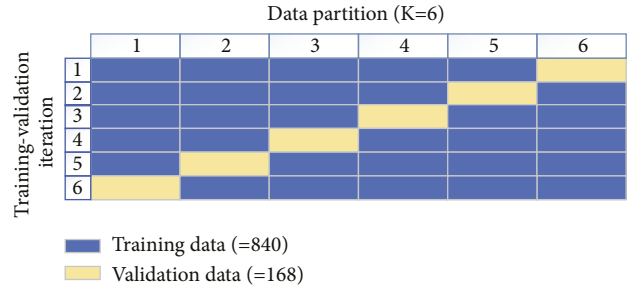

Figure 9: Six-fold cross-validation.

iteration is carried out for six cycles. For each training-validation iteration, a different partition for training and validation is used. Therefore, each data is used once for validation and $K-1$ times for training. Finally, the model with the least cost of validation (best fitness) is considered the optimized FIS model, and it is this FIS model that is taken for checking with the test dataset.

3.6. FIS Model Tuning Using HGSA. The goal of FIS model parameter tuning is to obtain the best model parameters with the lowest prediction error by creating the best input-output mapping. The FIS model training or tuning has been formulated as optimization problem with the objective of finding the optimal FIS model parameters that minimize the mean square error (MSE) of prediction. MSE is used as a fitness function f that can be expressed as follows:

$$f = \frac{1}{N}\sum_{i=1}^{N}\left(Y_i^t - Y_i^p\right)^2, \tag{6}$$

where Y_i^t is the target/desired output, Y_i^p is the predicted output of the FIS model for the i^{th} data point, and N is the number of data points. Y_i^p is the nonlinear function of input

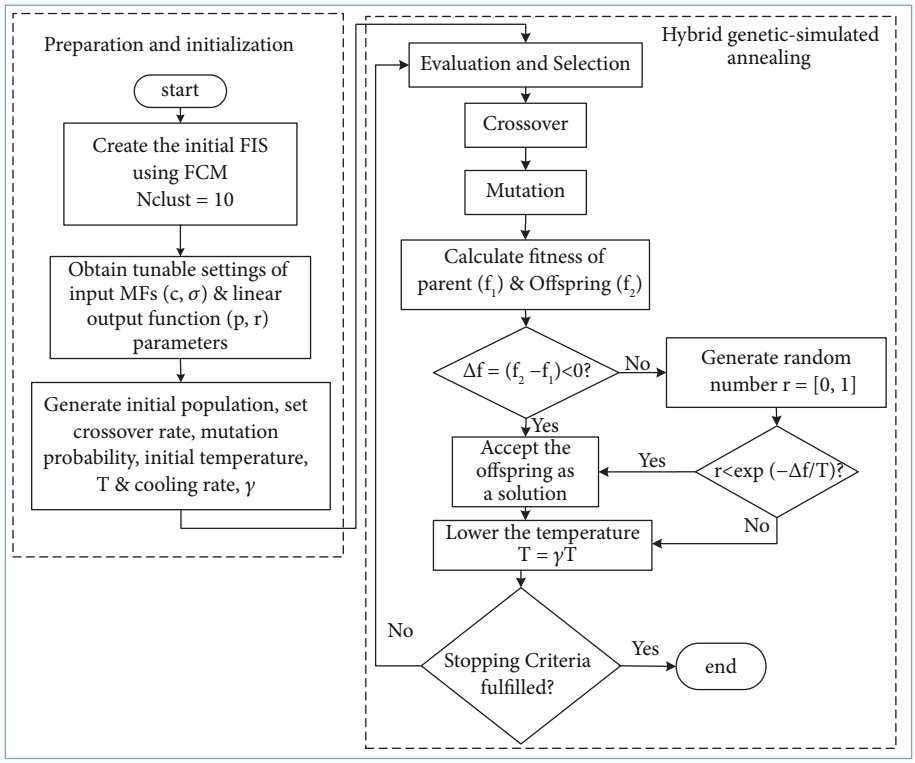

Figure 10: HGSA algorithm applied to tune fuzzy inference system parameters.

x, input MF parameters (c_i & σ_i), and linear output function parameters (p_i & r_i), and it can be expressed as follows:

$$Y_p^i = F(x, c_i, \sigma_i, p_i, r_i). \tag{7}$$

The optimization problem is to find c_i, σ_i, p_i, and r_i, which minimize f in (6). The HGSA algorithm presented in Figure 10 has been applied to obtain these parameters.

As shown in the flowchart, the initial FIS model, including its rule base, is generated in MATLAB using fuzzy c-means clustering (FCM), in which the whole training dataset is clustered into ten (Nclust = 10) clusters. The initial values of input MF parameters (c_i & σ_i) and output linear function parameters (p_i & r_i) are obtained and used for initialization along with other randomly generated initial values. Based on the fitness values, roulette wheel selection is applied to choose the parents for future crossover and mutation. Single point crossover and mutation are applied to create a new offspring. After the evaluation of fitness of parents f_1 and offsprings f_2, a change in fitness $\Delta f = f_2 - f_1$ is computed. If $\Delta f < 0$, the offspring will be directly accepted. Otherwise, a random number r between 0 and 1 is generated, and if $r < e^{-(\Delta f/T)}$, the new solution is accepted, otherwise discarded. Finally, the temperature is lowered according to the cooling rate γ. The process continues until the temperature freezes ($T \approx 0$).

3.7. Performance Evaluation. The trained FIS model has been tested using the unseen test data. The performance of the FIS model tuned by the HGSA algorithm is evaluated by root mean square error (RMSE) and Pearson's coefficient of correlation (R) evaluated using unseen test data. RMSE is applied to measure the deviation between values predicted by a model and the target values. RMSE can be computed as follows:

$$RMSE = \sqrt{\frac{1}{N}\sum_{i=1}^{N}\left(Y_t^i - Y_p^i\right)^2}, \tag{8}$$

where Y_t^i is the target output of instance i, Y_p^i is the actual output of the model, and N is the number of data points.Pearson's coefficient of correlation, R, known to be the best method of measuring the association between the variables of interest because it is based on the method of covariance [64, 65], is used to evaluate the performance of HGSA-FIS model by evaluating the correlation between the target and the predicted output. It can be computed as follows:

$$R = \frac{\sum_{i=1}^{N}\left(Y_t^i - \overline{Y_t}\right)\left(Y_p^i - \overline{Y_p}\right)}{\sqrt{\sum_{i=1}^{N}\left(Y_t^i - \overline{Y_t}\right)^2\left(Y_p^i - \overline{Y_p}\right)^2}}. \tag{9}$$

Y_t^i and Y_p^i are the individual values of the target and actual output, respectively, $\overline{Y_t}$ and $\overline{Y_p}$ are the sample mean of Y_t and Y_p, respectively, and N is the sample size. The value of R varies between −1 and 1 for the perfect negative and positive relationship, and 0 means no correlation between

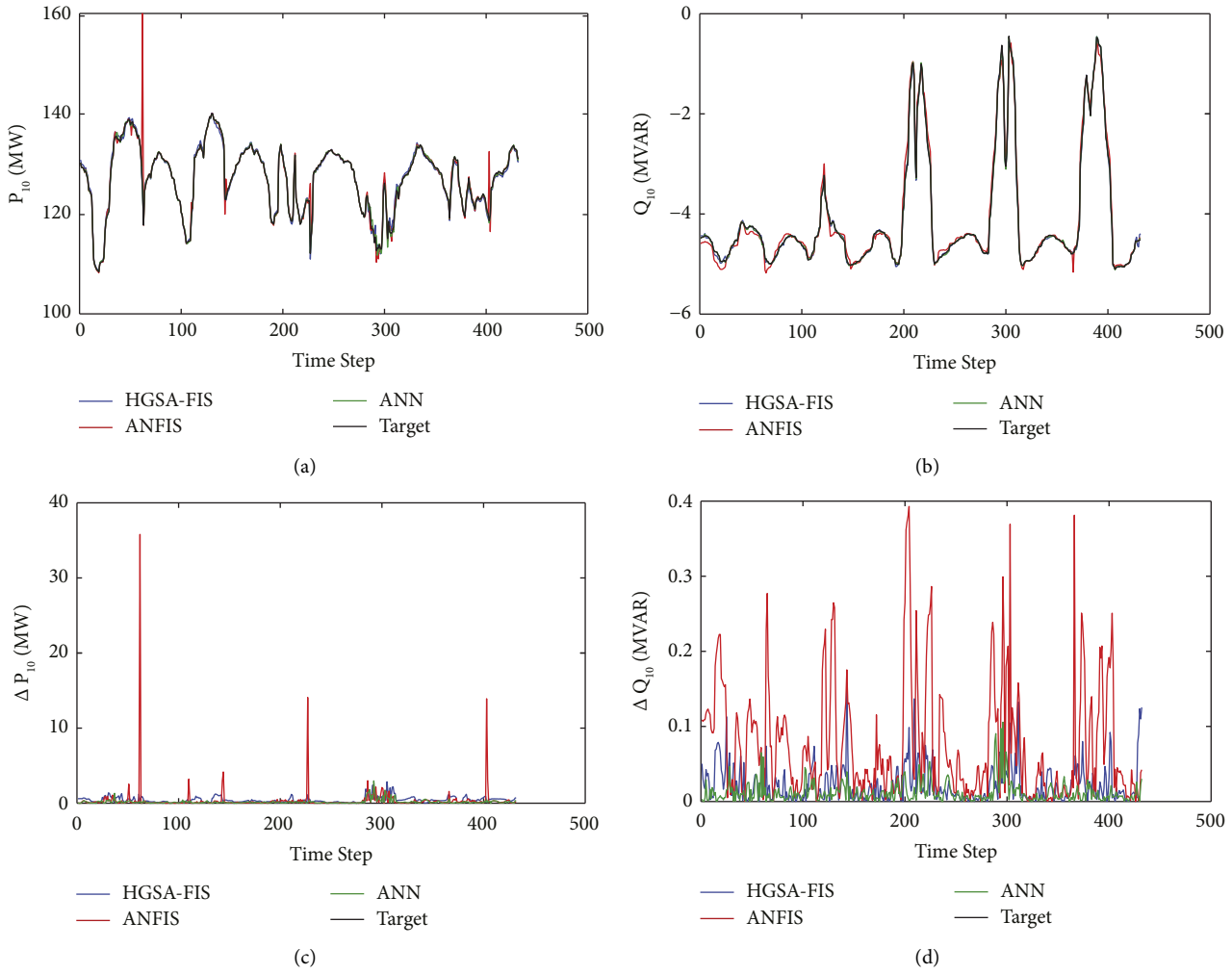

Figure 11: Comparison of prediction accuracy of HGSA-FIS, ANFIS, and ANN models in predicting tie-line L10 power flows: (a) P_{10}, (b) Q_{10}, (c) APE $|\Delta P_{10}|$, and (d) APE $|\Delta Q_{10}|$.

the two variables. A perfectly trained FIS prediction model gives R value very close to 1.

Besides the overall performance of the prediction models, to measure the performance of the prediction models for specific operating conditions or grid states, the absolute prediction error (APE) defined in (10) is used.

$$APE_i = \left|Y_t^i - Y_a^i\right|. \tag{10}$$

An ideal static equivalent is expected to provide power flow analysis results in the internal system closer to the results obtained before equivalencing. The power flow analysis results include, but not limited to, percentage line loading (%), buses voltage magnitude (p.u or kV), line active (MW), and reactive (MVAR) power flows. Thus, the performance of HGSA-FIS-based equivalent has also been evaluated by performing the time-series power flow analysis of the internal power system before and after equivalencing. The maximum absolute deviation (MAD) and weighted average percentage error (WAPE) are used to measure the deviation of percent line loading, bus voltage, and active and reactive power flow of transmission lines in the internal system after equivalents are attached from that obtained by power flow analysis of the full three area system before reduction. MAD and WAPE can be computed from equations (11) and (12), respectively.

$$MA\ D = \max\left|A_i - C_i\right|, i = 1, 2, \ldots, N, \tag{11}$$

$$WAPE = \frac{\sum_{i=1}^{N}\left|A_i - C_i\right|}{\sum_{i=1}^{N}\left|A_i\right|} * 100\%, \tag{12}$$

where A_i represents either the bus voltage, line active/reactive power flow, or percentage line loading obtained from the unreduced base system. C_i represents the same parameters obtained after equivalencing, and N is the number of test grid states considered for the evaluation.

4. Results and Discussion

As mentioned in the previous sections, input MF and output linear function parameters of the FIS model that have been tuned using the HGSA algorithm to provide optimized

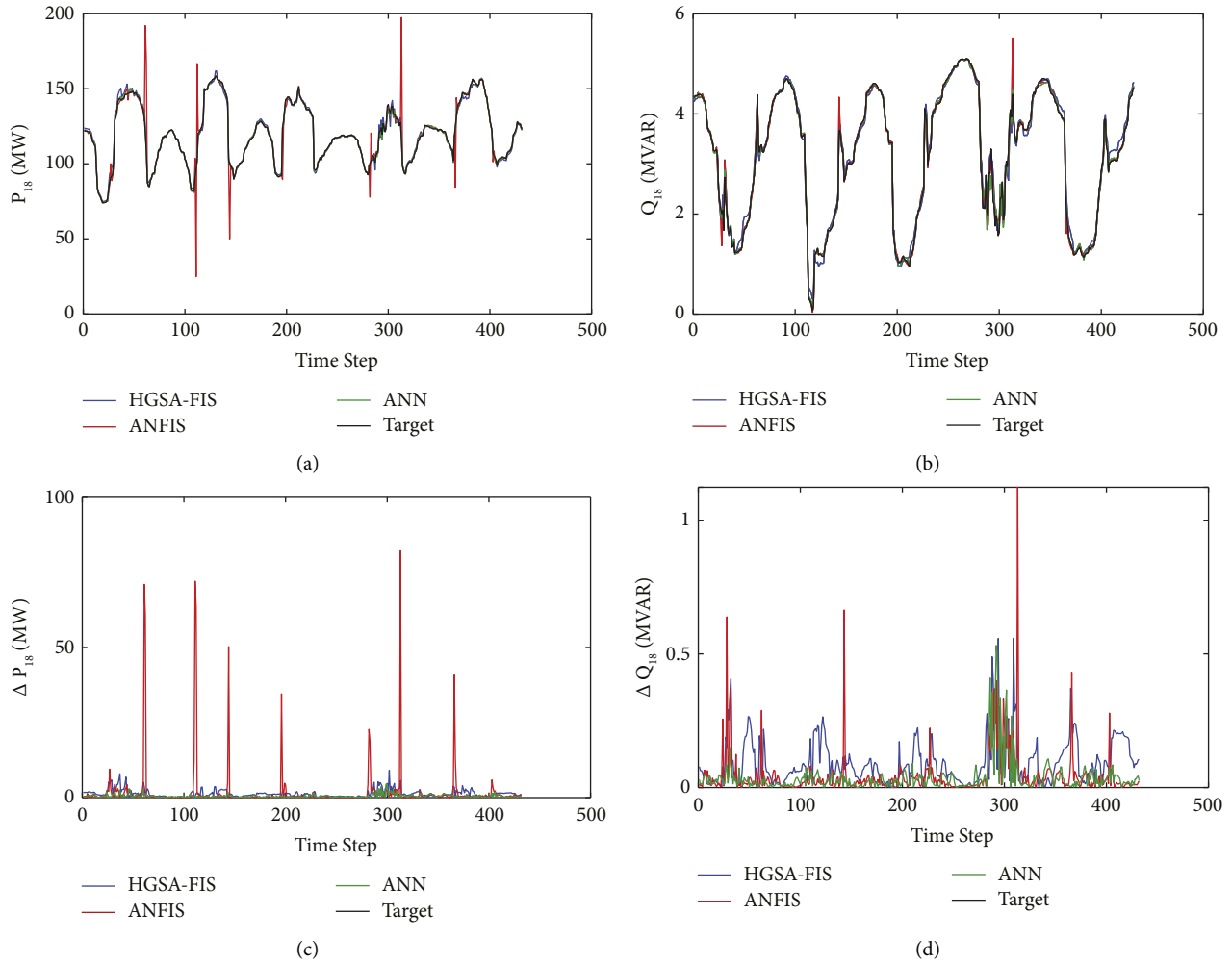

FIGURE 12: Comparison of prediction accuracy of HGSA-FIS, ANFIS, and ANN models in predicting tie-line L18 power flows: (a) P_{18}, (b) Q_{18}, (c) APE $|\Delta P_{18}|$, and (d) APE $|\Delta Q_{18}|$.

prediction performance, and the resulting FIS model is referred in this paper as HGSA-FIS. The performance of HGSA-FIS has been evaluated using different metrics on the basis of the following: (1) accuracy in predicting tie-line flows using APE, RMSE, and R and (2) power flow errors after HGSA-FIS equivalents are attached to the internal system. The base values of tie-line flows are obtained from the time-series power flow analysis of RTS-GMLC test system under varying operating conditions. Equivalents based on ANFIS trained by back-propagation and least square methods and ANN trained by back-propagation gradient-descent algorithm are used for comparison. The evaluation of HGSA-FIS model training results, performance evaluation of HGSA-FIS equivalents, and practical implementation requirements of the proposed equivalencing approach are presented in subsequent subsections.

4.1. HGSA-FIS Training Results. As explained in Section 3, there are eight FIS models to predict active and reactive power flows across four tie-lines. Each FIS model is tuned independent of the other with separate dataset prepared for each one of them. After repeated tuning of HGSA-FIS, its performance has been checked with test dataset. The prediction results of HGSA-FIS have been compared with two existing prediction tools, i.e., ANFIS and ANN. RMSE, APE, and R have been used to compare the performance of HGSA-FIS, ANFIS, and ANN.

As shown in Figures 11–14, HGSA-FIS performed well in predicting the tie-line power flows. It performs well close to ANN better than ANFIS.

The prediction performance of HGSA-FIS as compared to ANFIS and ANN measured by APE at each time step of the grid operation is shown in Figures 11–14(d), respectively, for tie-lines active and reactive power flows. As shown in the respective figures, the APE of HGSA-FIS-based prediction is generally lower than that of ANFIS and higher than ANN. Though it performed well to most of the test points, ANFIS experiences high APE values at some instances, as shown in Figures 11–14(d). It could not make smooth generalizations as compared to HGSA-FIS and ANN.

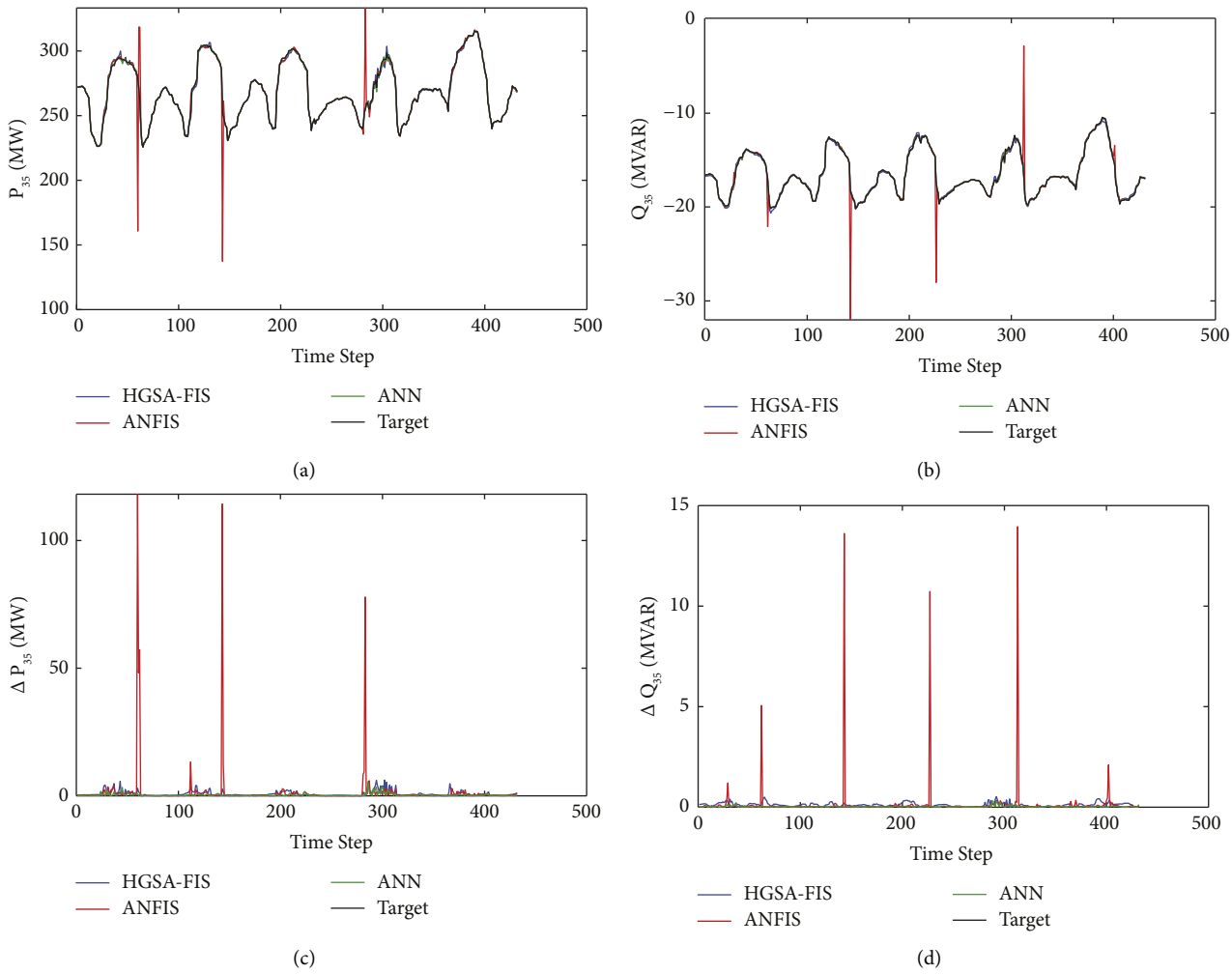

Figure 13: Comparison of prediction accuracy of HGSA-FIS, ANFIS, and ANN models in predicting tie-line L35 power flows: (a) P_{35}, (b) Q_{35}, (c) APE $|\Delta P_{35}|$, and (d) APE $|\Delta Q_{35}|$.

Table 3 presents the maximum absolute prediction error (MAPE) of HGSA-FIS, ANFIS, and ANN models in predicting the tie-lines active and reactive power flows. These values are extracted from the results presented in Figures 11–14(d). The MAPE observed by HGSA-FIS model is 34.81 MVAR and 11.01 MW in predicting Q_{102} and P_{102}, respectively.

The overall performance of the prediction models measured by RMSE (in MW or MVAR) and R is presented in Table 4. The maximum RMSE observed by HGSA-FIS is 7.5215 MVAR in predicting Q_{102} as compared to 9.8926 MVAR and 1.3082 MW of ANFIS and ANN, respectively.

In terms of Pearson's correlation coefficient (R), HGSA-FIS performed very well above 0.9955 to 0.9999, implying that the predicted and target values have high correlation, as shown in Figure 15(a) for the lowest R values and Figure 15(b) for the highest R values.

As shown in the figure, the HGSA-FIS model provides outputs very close to the target values for most of the test datasets.

4.2. Evaluation of Equivalents. After the prediction of values of dependent loads/injections, which represent the external grids, the equivalents are attached to boundary buses as shown in Figure 16.

Time series power flow analysis for unseen operating conditions has been carried out to evaluate the performance of the external equivalents. The deviation of line loading, line active, and reactive power flows and buses voltage magnitude in the internal system are observed and compared with those values obtained from unreduced three-area system.

The absolute deviation (AD) and weighted average percentage error (WAPE) are used to measure and compare the performance of HGSA-FIS, ANFIS, and ANN-based static equivalents. The maximum absolute deviations of percent line loading (%), voltage magnitude (p.u), active (MW), and reactive (MVAR) power flows are presented using bar charts shown in Figure 17. As it can be seen in the figure, the differences between HGSA-FIS- and ANN-based equivalents are not significant. The external equivalents based on ANFIS results in higher load flow deviations as compared to HGSA-FIS and ANN.

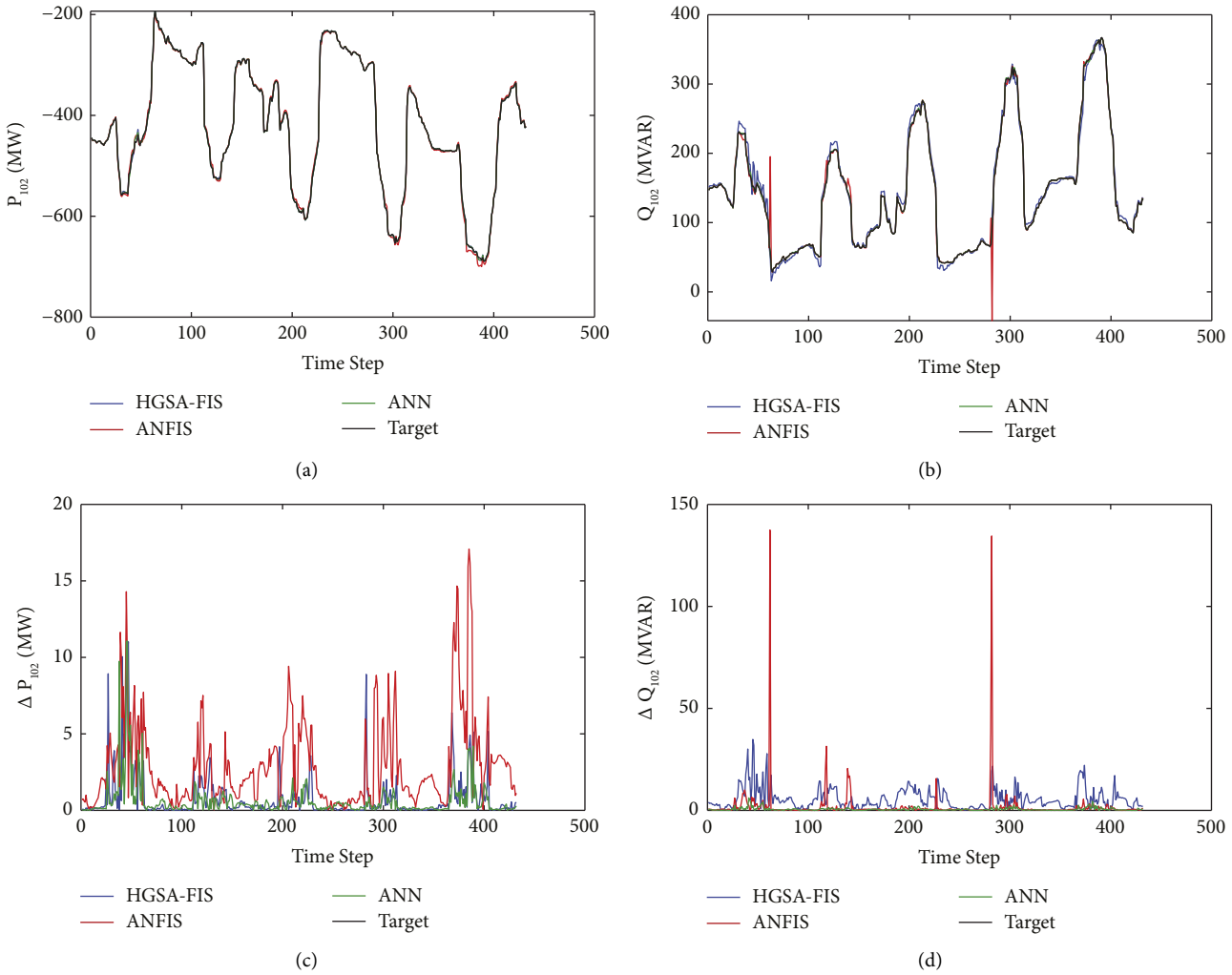

Figure 14: Comparison of prediction accuracy of HGSA-FIS, ANFIS, and ANN models in predicting tie-line L102 power flows: (a) P_{102}, (b) Q_{102}, (c) APE $|\Delta P_{102}|$, and (d) APE $|\Delta Q_{102}|$.

Table 3: Maximum APE of HGSA-FIS, ANFIS, and ANN models.

Target	APE (MW or MVAR)		
	HGSA-FIS	ANFIS	ANN
P_{10}	2.85	35.80	2.98
Q_{10}	0.16	0.39	0.11
P_{18}	9.07	82.20	4.45
Q_{18}	0.56	1.12	0.53
P_{35}	6.14	118.14	5.14
Q_{35}	0.52	13.95	0.32
P_{102}	11.01	17.08	11.08
Q_{102}	34.81	137.47	6.15

Table 4: Performance of HGSA-FIS, ANFIS, and ANN.

Target	(RMSE, R)		
	HGSA-FIS	ANFIS	ANN
P_{10}	(0.5850, 0.9962)	(2.0349, 0.9555)	(0.3256, 0.9988)
Q_{10}	(0.0341, 0.9996)	(0.1090, 0.9659)	(0.0181, 0.9999)
P_{18}	(1.8075, 0.9958)	(8.5886, 0.9171)	(0.7589, 0.9993)
Q_{18}	(0.1274, 0.9955)	(0.1005, 0.9970)	(0.0705, 0.9985)
P_{35}	(1.3214, 0.9982)	(9.5633, 0.9141)	(0.6292, 0.9996)
Q_{35}	(0.1498, 0.9980)	(1.1068, 0.9072)	(0.0474, 0.9998)
P_{102}	(1.6627, 0.9999)	(4.0768, 0.9995)	(1.3082, 0.9999)
Q_{102}	(7.5215, 0.9962)	(9.8926, 0.9932)	(0.8946, 0.9999)

The maximum of maximum absolute deviations for percent line loading, bus voltage, active power flow, and reactive power flow obtained from HGSA-FIS-, ANFIS-, and ANN-based equivalents is presented in Table 5.

As presented in the table, HGSA-FIS-based equivalent results in bus voltage deviation are lower than 0.0006 p.u (≡ 0.083 kV in 138 kV grid), and a deviation in percent line loading is less than 1.74%. ANN-based equivalent provides

Table 5: Maximum deviation of HGSA-FIS-, ANFIS-, and ANN-based equivalents.

Grid parameter	Maximum APE		
	HGSA-FIS	ANFIS	ANN
Voltage	0.0006 (bus 102)	0.005 (bus 102)	0.0004 (bus 109)
Active power flow (line 25)	8.82	81.46	4.85
Reactive power flow (line 25)	2.4	23.48	1.25
Percentage line loading	1.74 (line 25)	19.3 (line 9)	1.60 (line 9)

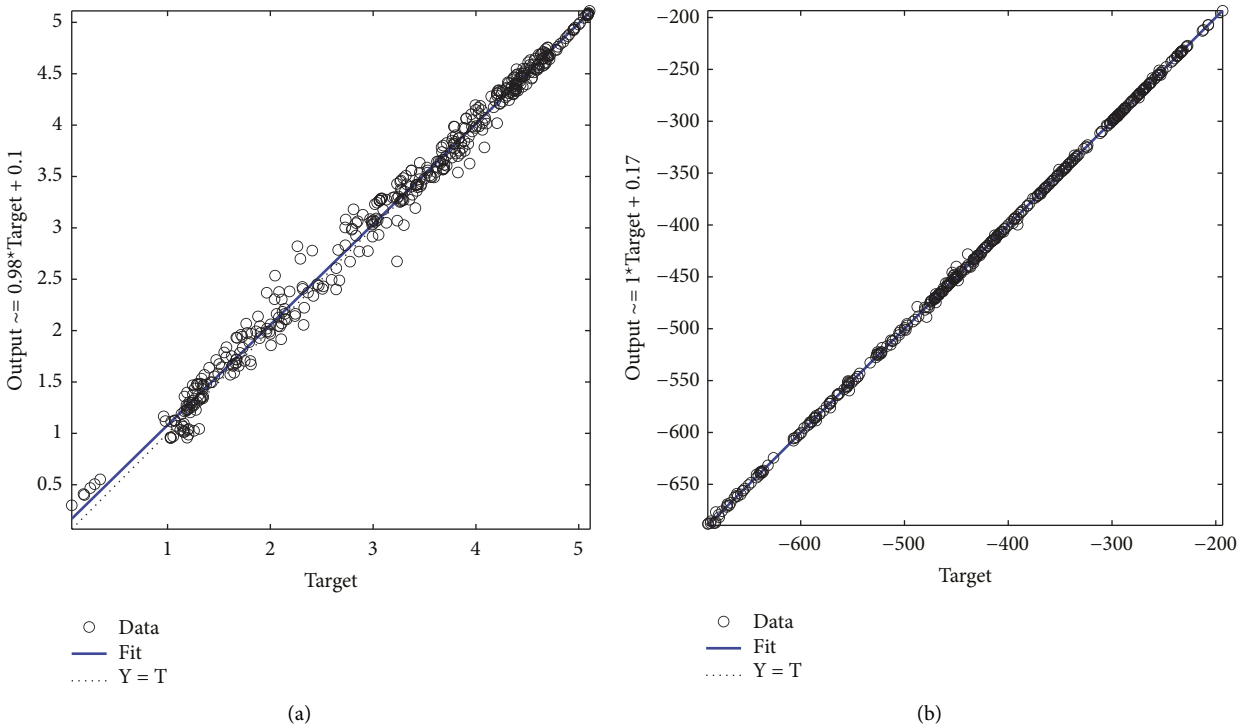

Figure 15: Similarity between target and predicted output. (a) $R = 0.9955$ for Q_{18}. (b) $R = 0.9999$ for Q_{102}.

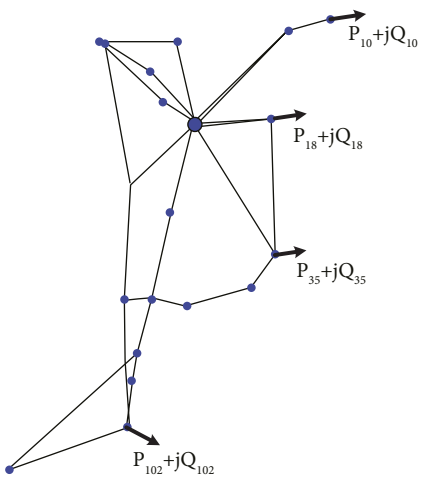

Figure 16: Internal area with external equivalents.

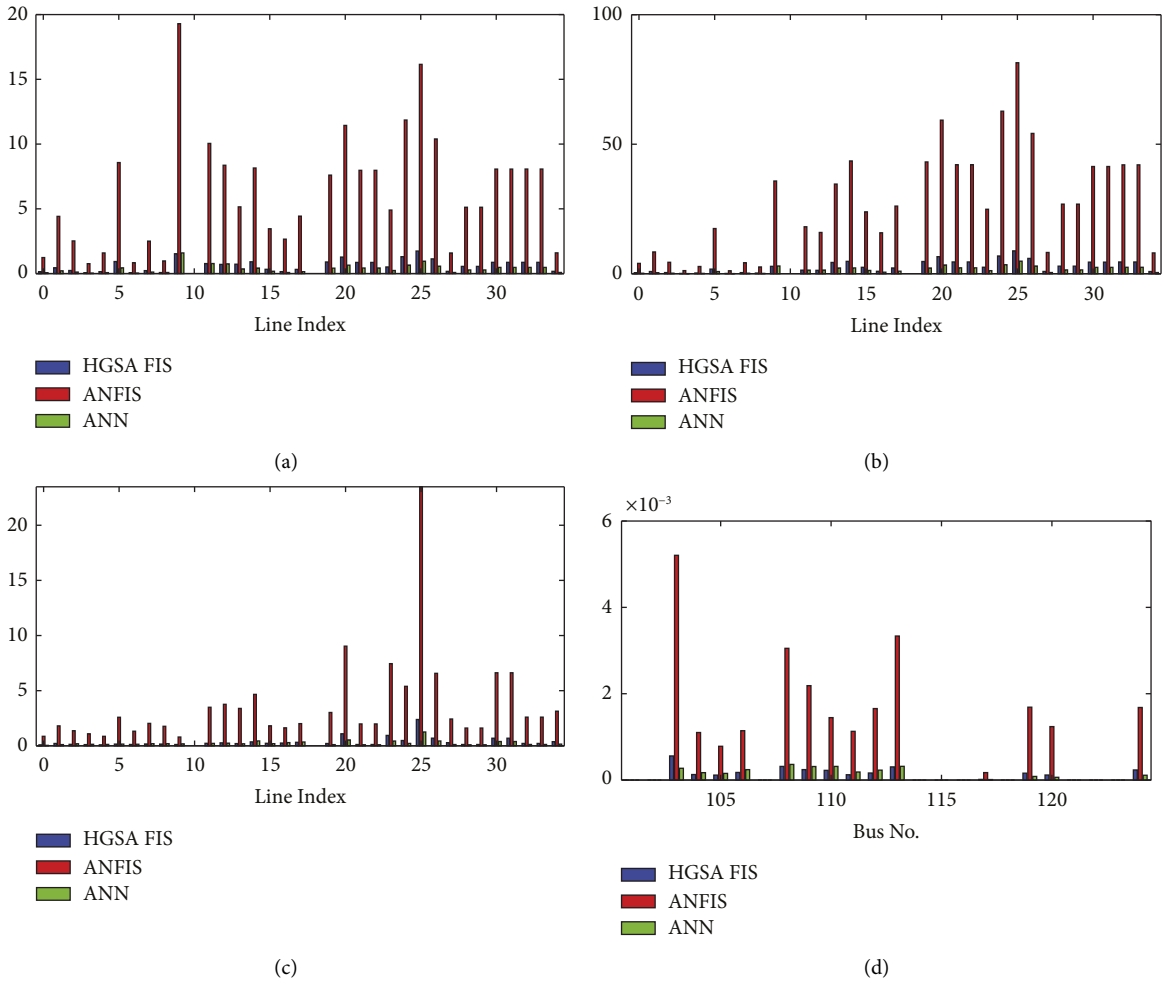

Figure 17: Maximum absolute deviations of (a) percent line loading (%), (b) lines active power flow (MW), (c) lines reactive power flow (MVAR), and (d) buses voltage (p.u).

lower maximum deviations than that obtained from HGSA-FIS-based equivalent.

Hence, HGSA-FIS- and ANN-based equivalents can be implemented to reduce the multiarea power system in static security assessment. However, since ANFIS-based equivalent results in a deviation of percent line loading by 19.3%, it cannot be used for static security assessment as it leads to wrong conclusions in power flow analysis and static security assessment.

To understand the overall deviation of the grid parameters for each equivalent technique for test grid states, the weighted average percentage error (WAPE) has been computed. The WAPE of these parameters obtained from the power flow analysis of the internal system after equivalents based on HGSA-FIS, ANFIS, and ANN are attached to the internal system is shown in Figure 18.

Table 6 presents the maximum WAPE values of buses voltage, active and reactive power flows, and percentage line loading with respective components.

4.3. Implementation Requirements. From the results obtained from the evaluation of HGSA-FIS-based equivalent approach in terms of prediction accuracy of tie-line flows (APE, RMSE, and R) and load flow errors (AD and WAPE), the proposed HGSA-FIS approach is positioned well above ANFIS and close to ANN. The results of its performance evaluation demonstrate that it can be successfully implemented to obtain the static equivalent of external systems in the static security assessment of multiarea power systems. To implement the proposed static equivalent approach in practical multiarea power systems, the responsible operators should do the following:

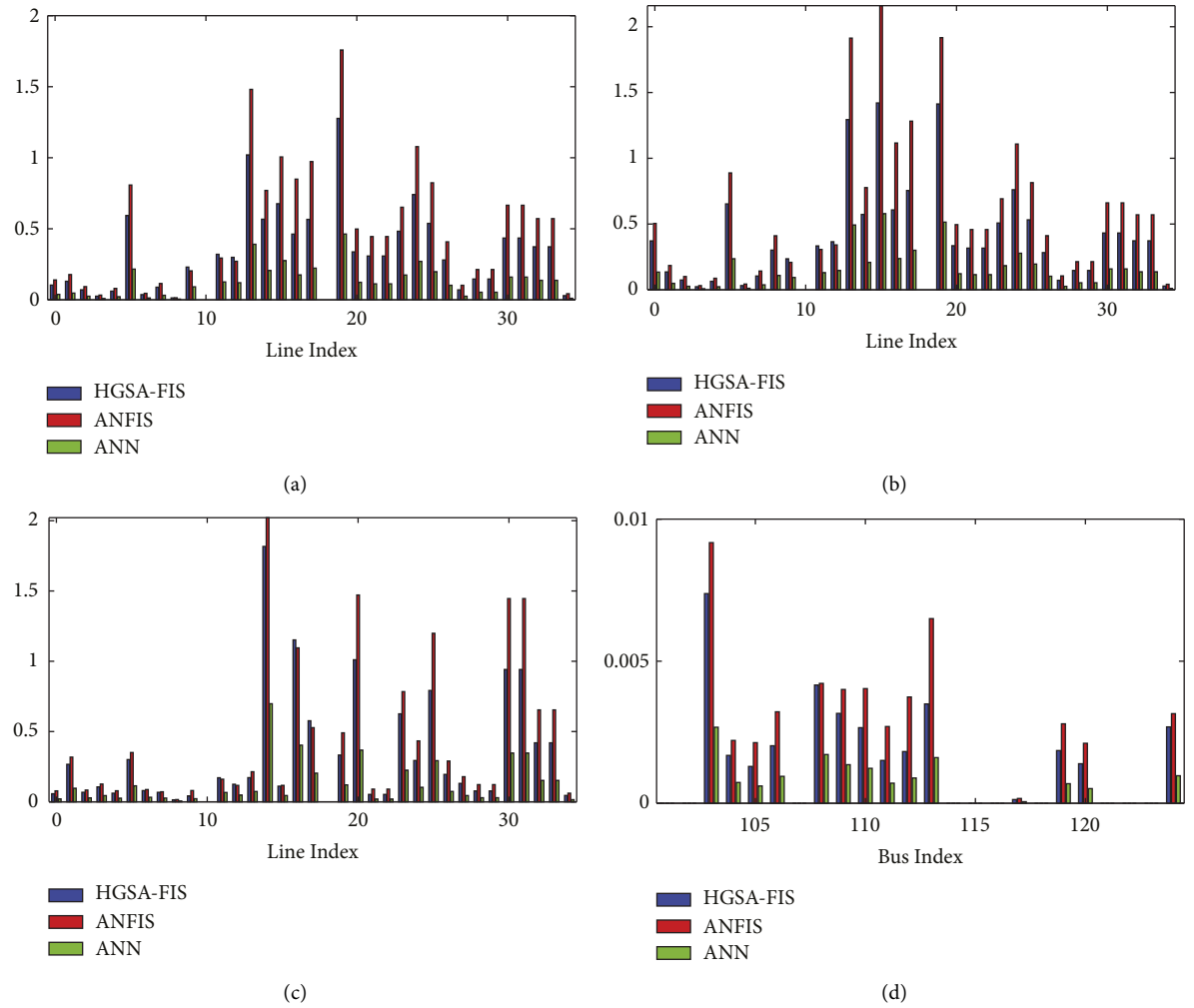

Figure 18: Performance of equivalents as measured by WAPE (%), (a) percent line loading deviation, (b) lines active power flow deviation, (c) lines reactive power flow deviation, and (d) buses voltage deviation.

Table 6: Maximum WAPE (%) of HGSA-FIS-, ANFIS-, and ANN-based equivalents.

Grid parameter	Maximum WAPE (%)		
	HGSA-FIS	ANFIS	ANN
Voltage (bus 103)	0.007	0.009	0.003
Active power flow (line 15)	1.42	2.16	0.58
Reactive power flow (line 14)	1.82	2.02	0.7
Percentage line loading (line 19)	1.28	1.76	0.46

(i) update the equivalent model when major changes happen to anyone of the connected power systems. The changes may be the addition or removal of generation power plants, high power loads, HVAC, or HVDC transmission lines.

(ii) exchange the generation and load demand forecasting data of selected REGs and loads. The proposed approach does not require the exchange of detail grid operation data between the neighboring interconnected areas.

5. Conclusion

External static equivalent helps to ease the power flow study and static security evaluation in multiarea systems. Any disturbance or change in the internal and external power systems is reflected by a change in the tie-line power flow. Therefore, the ability to find tie-line power flow flexibly with minimal information from the neighboring external system is essential. In this paper, HGSA-FIS model is proposed to predict tie-line flows, representing the static conditions of

the external power system. The proposed model requires only the active power output of a few REGs and load demands to make the required predictions. The developed model has been tested with sample scenarios generated by the time-series power flow analysis of the RTS-GMLC system. The prediction performance of the HGSA-FIS has been evaluated using APE, RMSE, and *R*. The results demonstrate that the proposed model performs close to ANN and better than ANFIS. Furthermore, the power flow analysis of the internal system before and after equivalencing reveals that the proposed equivalent approach is sufficient to represent the external systems for power flow study and static security assessment of internal systems. The proposed equivalent approach can be successfully implemented practically if it can be updated upon major grid changes in any of the connected systems and operators are willing to exchange the forecast data of a few REG power outputs and load demands. In the future, a similar equivalencing approach can be extended to obtain external equivalents during a contingency in the external system by incorporating the switching states of the lines as an input attribute to train the FIS model.

Data Availability

The grid network data and time-series generation and loaddemand data is available at GitHub Repository [60].

Conflicts of Interest

The authors declare that they have no conflicts of interest regarding the publication of this paper.

Acknowledgments

The research work presented in this manuscript is funded by Pan African University Institute for Basic Sciences, Technology and Innovation (PAUSTI), Kenya.

References

[1] O. Alizadeh Mousavi, *On Voltage and Frequency Control in Multi-Area Power Systems Security*, EPFL, Ph.D. dissertation Switzerland, 2014.

[2] G. Hug-Glazmann, *Coordinated Power Flow Control to Enhance Steady-State Security in Power Systems*, ETH Zurich, Switzerland Ph.D. dissertation, 2008.

[3] R. A. G. Tinoco, J. A. Passos Filho, W. Peres, and R. M. Henriques, "A new particle swarm optimization-based methodology for determining online static security regions," *International Transactions on Electrical Energy Systems*, vol. 31, no. 3, 2021.

[4] K. Alcheikh-Hamoud, N. Hadjsaid, Y. Besanger, and J.-P. Rognon, *Decision Tree Based Filter for Control Area External Contingencies Screening*, in *Proceedings of the 2009 IEEE Bucharest PowerTech*, pp. 1–8, Bucharest, Romania, 2009.

[5] R. V. Angadi, S. B. Daram, and P. Venkataramu, *Analysis of Power System Security Using Big Data and Machine Learning Techniques*, in *Proceedings of the 2020 IEEE 17th India Council International Conference (INDICON). IEEE*, pp. 1–8, New Delhi, India, 2020.

[6] T. Kang, J. Yao, T. Duong, S. Yang, and X. Zhu, "A hybrid approach for power system security enhancement via optimal installation of flexible ac transmission system (facts) devices," *Energies*, vol. 10, no. 9, pp. 1305–1332, 2017.

[7] Z. Dong, P. Zhang, J. Ma et al., *Emerging Techniques in Power System Analysis*, Springer, USA, 2010.

[8] Z. Liu, J.-H. Menke, N. Bornhorst, and M. Braun, "Static grid equivalent models based on artificial neural networks," *IEEE Access*, vol. 9168546 pages, 2021.

[9] J. Machowski, A. Cichy, F. Gubina, and P. Omahen, "External subsystem equivalent model for steady-state and dynamic security assessment," *IEEE Transactions on Power Systems*, vol. 3, no. 4, pp. 1456–1463, 1988.

[10] O. Makela, *Methods to Assess and Manage Security in Interconnected Electrical Power Systems*, ETH Zurich, Switzerland Ph.D. dissertation, 2013.

[11] C.-N. Lu, K.-C. Liu, and S. Vemuri, "An external network modeling for on-line security analysis," in *Proceeding of the Conference Papers Power Industry Computer Application Conference*, pp. 220–224, IEEE, 1989.

[12] A. N. Al-Masri, M. Z. A. Ab Kadir, A. S. Al-Ogaili, and Y. Hoon, "Development of adaptive artificial neural network security assessment schema for malaysian power grids," *IEEE Access*, vol. 7180105 pages, 2019.

[13] K. Lo, L. Peng, J. Macqueen, A. Ekwue, and D. Cheng, "An extended ward equivalent approach for power system security assessment," *Electric Power Systems Research*, vol. 42, no. 3, pp. 181–188, 1997.

[14] A. P. Gupta, A. Mohapatra, and S. N. Singh, "Power system network equivalents: key issues and challenges," in *Proceedings of the TENCON 2018-2018 IEEE Region 10 Conference*, pp. 2291–2296, IEEE, Korea, 2018.

[15] J. Yu, M. Zhang, W. Li, W. Yan, and X. Zhao, "Sufficient and necessary condition of sensitivity consistency in static equivalent methods," *IET Generation, Transmission & Distribution*, vol. 9, no. 7, pp. 603–608, 2015.

[16] W. Yan, C. Zhang, J. Tang, W. Qian, S. Li, and Q. Wang, "A black-box external equivalent method using tie-line power mutation," *IEEE Access*, vol. 7, pp. 11997–12005, 2019.

[17] I. S. Saeh and M. W. Mustafa, "Artificial neural network for power system static security assessment: a survey," *Jurnal Teknologi*, vol. 66, no. 1, 2013.

[18] F. S. Sevilla, "Evaluation of Static Network Equivalent Models for N-1 Line Contingency Analysis," in *Proceedings of the 2022 4th Global Power, Energy And Communication Conference (GPECOM)*, pp. 328–333, IEEE, Turkey, 2022.

[19] D. Degtiarev, S. Danilov, A. Kovalenko, A. Voloshin, and E. Voloshin, "Algorithm for generating the equivalent power system according to pmu," in *Proceedings of the 2022 4th Global Power, Energy and Communication Conference (GPECOM)*, pp. 444–448, IEEE, Turkey, 2022.

[20] M. Gholami, M. J. Sanjari, M. Safari, M. Akbari, and M. R. Kamali, "Static security assessment of power systems: a review," *International Transactions on Electrical Energy Systems*, vol. 30, no. 9, pp. 1–23, 2020.

[21] I. Pavic, Z. Hebel, and M. Delimar, "Power system equivalent based on an artificial neural network," in *Proceedings of the 23rd International Conference on Information Technology Interfaces*, pp. 359–365, IEEE, 2001.

[22] A. Larsson, A. Germond, and B. Zhang, "Application of neural networks to the identification of steady state equivalents of external power systems," in *Proceedings of the 2006*

International Conference on Power System Technology, IEEE, China, pp. 1–6, 2006.

[23] J.-H. Menke, M. Dipp, Z. Liu, C. Ma, F. Schäfer, and M. Braun, "Applications of artificial neural networks in the context of power systems," in *Artificial Intelligence Techniques for a Scalable Energy Transition*, pp. 345–373, Springer, USA, 2020.

[24] M. Yesil and E. Irmak, "A new bus reduction approach based on extended rei model," in *Proceedings of the 2022 4th Global Power, Energy and Communication Conference (GPECOM)*, pp. 400–405, IEEE, Turkey, 2022.

[25] H. Qu, M. Li, X. Yang, and P. Zhang, "Practical equivalent method of power network based on psasp short-circuit calculation program," *Energy and Power Engineering*, vol. 09, no. 04, pp. 683–692, 2017.

[26] T. Chung and F. Ying, "An ann-based network equivalent approach for power system on-line voltage security assessment," in," *POWERCON'98. 1998 International Conference on Power System Technology. Proceedings (Cat. No. 98EX151)*, IEEE, vol. 2, , pp. 1504–1507, 1998.

[27] P. Wang, Z. Zhang, Q. Huang, X. Tang, and W.-J. Lee, "Robustness-improved method for measurement-based equivalent modeling of active distribution network," *IEEE Transactions on Industry Applications*, vol. 57, no. 3, pp. 2146–2155, 2021.

[28] J. B. Ward, "Equivalent circuits for power-flow studies," *Electrical Engineering*, vol. 68, no. 9, p. 794, 1949.

[29] Digsilent Power Factory, *Digsilent Powerfactory 15 User Manual*, DIgSILENT GmbH, Germany, 2013.

[30] *Power World Corporation*, Power World Simulator User's Guide Version 13, Austin, USA, 2007.

[31] L. Thurner, A. Scheidler, F. Schafer et al., "Pandapower-an open-source Python tool for convenient modeling, analysis, and optimization of electric power systems," *IEEE Transactions on Power Systems*, vol. 33, no. 6, pp. 6510–6521, 2018.

[32] F. Ying and T. Chung, "An innovative fast voltage security assessment based on a hybrid ann external equivalent approach," in *IEEE Power Engineering Society Winter Meeting. Conference Proceedings (Cat. No. 00CH37077)*vol. 2, , pp. 987–992, IEEE, 2000.

[33] J. Yu, M. Zhang, and W. Li, "Static equivalent method based on component particularity representation and sensitivity consistency," *IEEE Transactions on Power Systems*, vol. 29, no. 5, pp. 2400–2408, 2014.

[34] P. Dimo, *Nodal Analysis of Power Systems*, International Scholarly Book Services, Inc, Forest Grove, OR, 1975.

[35] S. C. Savulescu, "Equivalents for security analysis of power systems," *IEEE Transactions on Power Apparatus and Systems*, vol. PAS-100, no. 5, pp. 2672–2682, 1981.

[36] J. Stadler and H. Renner, "Application of dynamic rei reduction," in *IEEE PES ISGT Europe 2013*, pp. 1–5, IEEE, USA, 2013.

[37] Z. Liu, N. Bornhorst, S. Wende-von Berg, and M. Braun, "A grid equivalent based on artificial neural networks in power systems with high penetration of distributed generation with reactive power control," in *NEIS 2020; Conference on Sustainable Energy Supply and Energy Storage Systems*, pp. 1–7, VDE, 2020.

[38] Y. Jilai and L. Zhuo, "Artificial neural networks based steady state equivalents of power systems," in *Proceedings of the First International Forum on Applications of Neural Networks to Power Systems*, pp. 174–177, IEEE, WA, USA, 1991.

[39] C. Zheng, S. Wang, Y. Liu et al., "A novel equivalent model of active distribution networks based on lstm," *IEEE Transactions on Neural Networks and Learning Systems*, vol. 30, no. 9, pp. 2611–2624, 2019.

[40] L. Wehenkel, "Machine learning approaches to power-system security assessment," *IEEE Expert*, vol. 12, no. 5, pp. 60–72, 1997.

[41] J. Kacprzyk and W. Pedrycz, *Springer Handbook of Computational Intelligence*, Springer, USA, 2015.

[42] M. M. Abdulgader, *Bio Inspired Evolutionary Fuzzy System for Data Classification*, The University of Toledo, USA, 2019.

[43] V. Ojha, A. Abraham, and V. Snášel, "Heuristic design of fuzzy inference systems: a review of three decades of research," *Engineering Applications of Artificial Intelligence*, vol. 85, pp. 845–864, 2019.

[44] M. Sugeno, "Fuzzy identification of systems and its applications to modeling and control," *IEEE transactions on systems, man, and cybernetics*, vol. SMC-15, no. 1, pp. 116–132, 1985.

[45] G. Chen and T. T. Pham, *Introduction to Fuzzy Sets, Fuzzy Logic, and Fuzzy Control Systems*, CRC Press, UK, 2000.

[46] H. Hellendoorn and D. Driankov, *Fuzzy Model Identification: Selected Approaches*, Springer Science & Business Media, USA, 2012.

[47] C.-H. Wang, C.-J. Tsai, T.-P. Hong, and S.-S. Tseng, "Fuzzy inductive learning strategies," *Applied Intelligence*, vol. 18, no. 2, pp. 179–193, 2003.

[48] Y. Yih, "Constructing a fuzzy rule system from examples," *Integrated Computer-Aided Engineering*, vol. 6, no. 3, pp. 213–222, 1999.

[49] J.-S. Jang, "Anfis: adaptive-network-based fuzzy inference system," *IEEE transactions on systems, man, and cybernetics*, vol. 23, no. 3, pp. 665–685, 1993.

[50] T. Yasukawa, "A fuzzy-logic-based approach to qualitative modeling," *IEEE Transactions on Fuzzy Systems*, vol. 1, no. 1, pp. 7–31, 1993.

[51] F. Guély, R. La, and P. Siarry, "Fuzzy rule base learning through simulated annealing," *Fuzzy Sets and Systems*, vol. 105, no. 3, pp. 353–363, 1999.

[52] Z. Akyürek, "Fuzzy model tuning using simulated annealing," *Expert Systems with Applications*, vol. 38, no. 7, pp. 8159–8169, 2011.

[53] U. Misra and C. Bloebaum, "A parallel hybrid genetic simulated annealing algorithm for large-scale constrained optimization," in *Proceedings of the 9th AIAA/ISSMO Symposium on Multidisciplinary Analysis and Optimization*, p. 5578, Atlanta, Georgia, 2002.

[54] X. Liang and Z. Du, "Genetic algorithm with simulated annealing for resolving job shop scheduling problem," in *Proceedins of the 2020 IEEE 8th International Conference on Computer Science and Network Technology (ICCSNT)*, pp. 64–68, IEEE, Dalian, 2020.

[55] K. Liu, W. Sheng, and Y. Li, "Research on reactive power optimization based on adaptive genetic simulated annealing algorithm," in *Proceedings of the 2006 International Conference on Power System Technology*, pp. 1–6, IEEE, MALAYSIA, 2006.

[56] R. Uma Maheswari and D. Jeya Mala, "Combined genetic and simulated annealing approach for test case prioritization," *Indian Journal of Science and Technology*, vol. 8, no. 35, p. 1, 2015.

[57] X. Xie, "Genetic algorithm and simulated annealing: a combined intelligent optimization method and its application to subsynchronous damping control in electrical power transmission systems," *Simulated Annealing: Advances, Applications and Hybridizations*, p. 245, 2012.

[58] C. Barrows, E. Preston, A. Staid et al., "The ieee reliability test system: a proposed 2019 update," *IEEE Transactions on Power Systems*, vol. 35, no. 1, pp. 119–127, 2020.

[59] C. Grigg, P. Wong, P. Albrecht et al., "The ieee reliability test system-1996. a report prepared by the reliability test system task force of the application of probability methods subcommittee," *IEEE Transactions on Power Systems*, vol. 14, no. 3, pp. 1010–1020, 1999.

[60] C. Barrows, "Reliability test system of grid moderenization laboratory consortium(rts-gmlc)," 2019, https://github.com/GridMod/RTS-GMLC.

[61] S. Abe, *Pattern Classification: Neuro-Fuzzy Methods and Their Comparison*, Springer Science & Business Media, USA, 2012.

[62] I. Guyon and A. Elisseeff, "An introduction to variable and feature selection," *Journal of Machine Learning Research*, vol. 3, pp. 1157–1182, 2003.

[63] W. Yang, K. Wang, and W. Zuo, "Neighborhood component feature selection for high-dimensional data," *Journal of Computers*, vol. 7, no. 1, pp. 161–168, 2012.

[64] D. Nettleton, *Commercial Data Mining: Processing, Analysis and Modeling for Predictive Analytics Projects*, Elsevier, Netherlands, 2014.

[65] S. Boslaugh, *Statistics in a Nutshell: A Desktop Quick Reference*, O'Reilly Media, Inc.", California, 2012002E.